Cellular/Molecular

alx, a Zebrafish Homolog of *Chx10*, Marks Ipsilateral Descending Excitatory Interneurons That Participate in the Regulation of Spinal Locomotor Circuits

Yukiko Kimura, Yasushi Okamura, and Shin-ichi Higashijima

National Institutes of Natural Sciences, Okazaki Institute for Integrative Bioscience, and National Institute for Physiological Sciences, Myodaiji Okazaki, Aichi 444-8787, Japan

Recent molecular genetic studies suggest that the expression of transcription factors in the developing spinal cord helps determine the morphological and physiological properties of neurons. Using the zebrafish preparation, we have examined the properties of neurons marked by *alx*, a zebrafish homolog of mammalian *Chx10*. We performed morphological and physiological studies using transgenic zebrafish expressing fluorescent reporter constructs in cells that had at any time point expressed *alx* (*alx* neurons). Our data reveal that zebrafish *alx* neurons are all ipsilateral descending neurons that are positive for vesicular glutamate transporter 2, suggesting that they are glutamatergic excitatory interneurons. Patch recordings show that earlier-born neurons are active during stronger movements such as escapes and fast swimming (strong movement class), whereas later-born ones are involved in sustained weak swimming (weak movement class). Paired recordings between *alx* neurons and motoneurons show that neurons of the strong movement class make frequent monosynaptic excitatory connections onto motoneurons. Thus, neurons of this class are likely premotor interneurons that regulate motoneuron activity during escapes and fast swimming. We also show the existence of a monosynaptic connection between an *alx* neuron of the weak movement class and a motoneuron. Collectively, our data demonstrate that *alx* marks ipsilateral descending neurons that are involved in the regulation of motoneuron activity during forms of locomotion, such as escape and swimming.

Key words: **neural development; locomotion; spinal cord; zebrafish; Chx10; GFP**

Introduction

The ventral region of the spinal cord is responsible for locomotion. Studies in the cat have led to the classification of several spinal interneurons with roles in sensory/motor pathways (Jankowska, 1992). Knowledge of neuronal circuits responsible for locomotion has been further advanced in rodent preparations, in which, for example, several classes of commissural interneurons that are likely involved in locomotor control have been identified (Kiehn and Butt, 2003). Nonetheless, identifying functional subtypes of interneurons has been difficult because of the enormous complexity of mammalian spinal circuits.

Genetic markers have proven useful for the identification of functional classes of spinal interneurons. During development, five distinct classes of neurons (V0–V3 interneurons and motoneurons) are produced in the ventral spinal cord in chicks and mice (Briscoe et al., 2000). Neurons of each class are characterized by the expression of different transcription factors, such as Engrailed1 (En1) for V1 neurons. Early classes of interneurons are thought to represent separate functional groups of cells, with neurons of each class sharing several common features. For example, En1-positive neurons have been shown to comprise ipsilateral inhibitory neurons including Renshaw cells and Ia inhibitory neurons (Sapir et al., 2004; Alvarez et al., 2005).

Because developmental mechanisms are highly conserved across vertebrate species, it should also be possible to correlate neuronal types in anamniotic fishes and amphibians with classes of interneurons defined developmentally (V0–V3 neurons). Spinal motor circuits are best characterized in anamniotes such as lampreys and frog tadpoles, in which functional subtypes of interneurons are well identified (Roberts et al., 1998; Grillner, 2003). Less is known about spinal networks in zebrafish, but zebrafish are especially amenable to a combination of genetic, developmental, and physiological studies. We have been using the zebrafish preparation to relate interneuronal types to developmental markers. Our previous study (Higashijima et al., 2004a), together with a parallel study in tadpoles (Li et al., 2004), showed that En1 expression defined a single population of ipsilateral glycinergic inhibitory interneurons that were multifunctional, involved in both motor control and sensory gating during swimming.

These studies are important in several ways. First, the studies provide a complementary way of identifying previously defined subtypes of neurons. Second, key features of En1-positive neu-

Received Nov. 22, 2005; revised April 14, 2006; accepted April 15, 2006.

This work was supported in part by grants from the Ministry of Education, Science, Technology, Sports and Culture of Japan. We are grateful to K. Horikawa, H. Takeda, T. Kurata, T. Sato, and H. Okamoto for suggestions on experiments, to S. Otto for help with molecular biology experiments during the initial phase of this study, and to D. McLean for comments on this manuscript.

Correspondence should be addressed to Shin-ichi Higashijima, National Institutes of Natural Sciences, Okazaki Institute for Integrative Bioscience, Higashiyama 5-1, Myodaiji, Okazaki, Aichi 444-8787, Japan. E-mail: shigashi@nips.ac.jp.

DOI:10.1523/JNEUROSCI.4993-05.2006

 0270-6474/06/265684-14$15.00/0

rons are widely conserved between the aquatic vertebrates and mammals. Thus, the studies provide a bridge between cell types in the aquatic vertebrates and those of mammals. The studies also provide insight into the evolution of spinal circuits in vertebrates. One emerging view is that early V0–V3 subdivisions of neurons in the embryonic spinal cord represent a primitive ground state that undergoes further diversification during development and/or evolution (Goulding et al., 2002; Goulding and Pfaff, 2005). The results of the En1 study in zebrafish/tadpoles are consistent with this view.

In the work presented here, we have extended our analysis to *alx*, a zebrafish homolog of *Chx10* (Barabino et al., 1997). Chx10 in amniotes marks a subset of V2 neurons, called V2a neurons (Karunaratne et al., 2002). We have revealed that *alx* marks ipsilateral descending neurons that provide excitation to motoneurons during locomotion. These results suggest that Chx10-positive cells in amniotes may have similar properties and also be involved in motor control.

Materials and Methods

Generation of DNA constructs for expressing fluorescent proteins in alx*-positive cells.* An *alx*-positive bacterial artificial chromosome (BAC) was identified by blasting the *alx* cDNA sequence (Barabino et al., 1997) against the BAC sequences of the Sanger Institute (http://www.sanger.ac.uk/cgi-bin/blast/submitblast/d_rerio). The positive clone, zK27P3, which we obtained from RZPD (Berlin, Germany), had an ~143 kb insert, of which ~120 kb was upstream of the gene. To generate *alx* reporter constructs, we followed the method by Lee et al. (2001), which uses BAC homologous recombination system (a gift from N. Copeland, National Cancer Institute, Frederick, MD). To make a plasmid construct for a template of targeting DNA, we subcloned enhanced green fluorescent protein (EGFP), a poly(A) signal from the bovine growth hormone (BGH) gene, and a kanamycin resistant gene (Km^r) in this order in pBluescript-SK (Stratagene, La Jolla, CA). The EGFP, BGH poly(A), and Km^r sequences were from pEGFP-N1 (Clontech, Palo Alto, CA), pcDNA3 (Invitrogen, Carlsbad, CA), and pAd10SacBII (Incyte Genomics, Palo Alto, CA), respectively. The targeting DNA fragment for homologous recombination (5′ arm-EGFP-poly(A)-Km^r-3′ arm) was prepared by PCR. Fifty bases of *alx*-derived sequences were added to each of the PCR primers. The *alx*-derived sequences were: 5′ arm, 5′-GCGCCTCGGATGCCTGTGCACAGGGGACCGACTCGAAAGCAAAGAAGGGA-3′, which is located 18 base pairs (bp) upstream of the putative translation start site of the *alx* gene, and 3′ arm, 5′-TCAAAATCGCTGTGTGCCACCGAGAACGGGGGAAATAACAATCCACATCT-3′, which is located 43 bp downstream of the putative translation start site. For the Kaede construct (Ando et al., 2002), the EGFP sequence in the template plasmid DNA was replaced by Kaede (a gift from A. Miyawaki, RIKEN, Saitama, Japan). For the Discosoma red (DsRed) construct, loxP, DsRed, BGH poly(A), Km^r, loxP, EGFP, and simian virus 40 (SV40) poly(A) were subcloned in this order in pBluescript-SK. The upper and lower strands of loxP sequences (upper strand, 5′-CTAATAACTTCGTATAGCATACATTATACGAAGTTATATT-3′; lower strand, complementary to the upper strand) were chemically synthesized. DsRed (DsRed-Express) and SV40 poly(A) sequences were from the pDsRed-Express-N1 and pEGFP-N1 (both from Clontech), respectively. An 18 bp sequence derived from the *alx* gene (5′-TCGAAAGCAAAGAAGGGA-3′) was added in front of the first loxP site for subsequent PCR amplification. To increase efficiency of transgenesis, we inserted an I-SceI meganuclease recognition site (Thermes et al., 2002) into the BAC DNA by homologous recombination. For this purpose, a synthetic I-SceI sequence (5′-TAGGGATAACAGGGTAAT-3′) and an Amp^r sequence (PCR-derived from pBluescript-SK) were placed, in this order, in a pEGFP-N1-based plasmid vector. The I-SceI and Amp sequence were PCR-amplified with primers to each of which 50 base of BAC vector-derived sequences (5′-TTCTCTGTTTTTGTCCGTGGAATGAACAATGGAAGTCCGAGCTCATCGCT-3′ and 5′-ATGCGGCCGCAAGGGGTTCGCGTCAGCGGGTGTTGGCGGGTGTCGGGGCT-3′) were added as arms for subsequent homologous recombination. The backbone vector of the *alx* BAC (zK27P3) contains a loxP site. The arm sequences for the introduction of I-SceI (and Amp) were designed so that the insertion of the sequence would result in the deletion of the original loxP site in the backbone vector.

Generation of stochastic expression construct. For stochastic expression of Cre, plasmid DNA in which a Cre-coding sequence was inserted into the pCS2 vector was used (a gift from T. Sato and H. Okamoto, RIKEN). The pCS2 has a cytomegalovirus promoter, which was used to drive Cre expression in a small number of cells in the transient expression system. For stochastic expression of monomeric red fluorescent protein (mRFP) (Campbell et al., 2002), a DNA construct in which mRFP (a gift from R. Tsien, University of California, San Diego, La Jolla, CA) was placed under a goldfish neural tubulin promoter (Hieber et al., 1998) was created and used.

Microinjection of DNA and generation of transgenic fish. Microinjection of DNA into zebrafish embryos was performed as described previously (Higashijima et al., 1997) using BAC DNA at 40–50 ng/μl and plasmid DNA at 20 ng/μl. BAC DNA was coinjected with I-SceI (Thermes et al., 2002). We obtained three lines for EGFP, two for Kaede, and two for DsRed. The expression pattern of fluorescent proteins in these lines was identical under epi-fluorescent microscopy. For each fluorescent protein, the brightest line was selected and used.

Antibody and in situ *hybridization staining.* The following primary antibodies were used: rabbit anti-Engrailed (a gift from A. Joyner, Skirball Institute, New York, NY); mouse monoclonal anti-NKX6.1 antibody (AB2024; a gift from I. Pedersen, Beta Cell Biology Consortium Antibody Core, Bagsvaerd, Denmark); rabbit anti-Lhx3 (Chemicon, Temecula, CA); mouse monoclonal anti-Islet1 (Isl1) antibodies (39.4D5 and 40.2D6; developed by T. Jessell and obtained from Developmental Studies Hybridoma Bank, University of Iowa, Iowa City, IA). The secondary antibodies used were: cyanine 5 (Cy5)-conjugated F(ab′)2 fragment of donkey anti-mouse IgG and Cy5-conjugated F(ab′)2 fragment of donkey anti-rabbit IgG antibodies (both from Jackson ImmunoResearch, West Grove, PA).

In situ hybridization was performed using a standard protocol. In older animals beyond 36 h postfertilization (hpf), the ventral region of the body was excised when the samples were in fixative (Higashijima et al., 2004b). For counting *alx*-positive cells, three segments (both sides of the spinal cord) from three fish were examined. For double *in situ* hybridization, one probe was labeled with digoxigenin and detected by alkaline phosphatase-conjugated anti-digoxigenin antibody and an HNPP fluorescent detection set (all reagents were from Roche, Penzberg, Germany). The other probe was labeled with fluorescein (Roche) and detected by peroxidase-conjugated anti-fluorescein antibody (Roche) and a TSA kit with Alexa Fluor 647 (Invitrogen) according to the manufacturer's instructions.

For *alx in situ* hybridization, the cDNA sequence between amino acid residues 230 and 489 was used as a template. The probes for vesicular glutamate transporters (vgluts; a mixture of *vglut2a* and *vglut2b*, called *VGLUT2.1* and *VGLUT2.2* formally) and glycine transporter2 (*glyt2*) have been described previously (Higashijima et al., 2004b). We cloned a zebrafish vesicular inhibitory amino acid transporter (*viaat*) gene in this study. Sequence information of the *viaat* gene was obtained by reconstituting four expressed sequence tag clones (CK143267, CN833360, CN503909, and CN838148). Based on the information, two PCR-primers, 5′-GAGGTCTAGACACCTGTCTCGTTTA-3′ and 5′-AGTATAACACCTAAACCACCAAAC-3′, were designed to amplify *viaat* cDNA. The resultant 1.6 kb fragment was subcloned and used as a template for *in situ* hybridization.

Photoconversion of Kaede. Photoconversion of Kaede was performed by broadly illuminating embryos with violet light (425DF60 nm) using a fluorescence dissecting microscope (FLIII; Leica, Wetzlar, Germany). Embryos in their chorions were illuminated for a few minutes until the fluorescence from Kaede became completely red. During illumination, the position of the embryos was occasionally changed with forceps.

Microscopic observation of zebrafish neurons. Observations of live and fixed tissue (except for samples after electrophysiological recording) were performed essentially as described previously (Hale et al., 2001; Higashijima et al., 2004b,c). For judging the presence or absence of GFP

in mRFP- or Texas Red-labeled cells, we were careful about the potential contamination of the mRFP/Texas Red signal into the GFP detection channel. Using GFP-negative cells (e.g., Rohon Beard sensory neurons) that had a strong fluorescence signal from mRFP/Texas Red, we set laser power, gain, off-set, etc. to levels in which the mRFP/Texas Red signal did not bleed into the GFP channel. All observations of mRFP/Texas Red were performed in cells whose mRFP/Texas Red fluorescence signal was weaker than that of the calibrated cells.

Retrograde labeling. Retrograde labeling of spinal interneurons was performed as described previously (Fetcho and O'Malley, 1995; Hale et al., 2001). Texas Red-conjugated dextran [molecular weight (M.W.), 3000; Invitrogen] was used as a dye.

Electrophysiological recordings. All the electrophysiological recordings were performed using *alx*:GFP (EGFP) fish at 52–62 hpf. Embryos were paralyzed by soaking them in 1 mg/ml of α-bungarotoxin (Sigma, St. Louis, MO) in water for 20–30 min. Embryos were then pinned to a Sylgard-lined glass-bottomed Petri dish with short pieces of fine tungsten wire pushed through the notochord. Embryos were then covered with extracellular recording solution that contained (in mM): 134 NaCl, 2.9 KCl, 1.2 $MgCl_2$, 2.1 $CaCl_2$, 10 HEPES, and 10 glucose, adjusted to pH 7.8 with NaOH (Drapeau et al., 1999). The skin in the middle region of the body was removed with a pair of forceps. Collagenase (0.03%; Sigma) in recording solution was applied to the preparation for 5–15 min. While embryos were in the collagenase solution, three to four segments (between the seventh and 12th segments) of muscle fibers that covered the spinal cord were carefully removed manually with a pair of fine (but not sharp) forceps. The collagenase treatment was omitted in preparations for ventral root (VR) recordings. For all electrophysiology experiments, the preparations were observed using a water immersion objective (40×; numerical aperture, 0.80; Olympus, Tokyo, Japan) on an upright microscope (BX51WI; Olympus) fitted with differential interference contrast optics.

A stimulation electrode was placed near the otolith. In the early phase of our experiments, the electrode was placed on the ipsilateral side in relationship to the recording side (top), whereas in the late phase, it was placed on the contralateral side (bottom). Approximately one-half of our recordings were made using contralateral stimulation. A stimulation strength of 5–15 V for a duration of 2–5 ms was used to elicit fictive motor behavior.

Extracellular recordings from motor nerves were performed as described by Masino and Fetcho (2005). Recording sites were typically two to six segments rostral from the patch-electrode recording site. Whole-cell recordings were performed as described by Higashijima et al. (2004a) with minor modifications. Slightly narrower tip diameter electrodes (20–40 MΩ in resistance) were used. For paired recordings between an *alx* neuron and a potential postsynaptic neuron, the second electrode was targeted to a cell located in the segment where the GFP-positive cell lay or in the segment just caudal to it. We recorded from cells located in the ventral motoneuron-enriched domain. We used two different patch solutions, #1 solution (in mM: 125 K-gluconate, 2 $MgCl_2$, 10 HEPES, 10 EGTA, and 4 Na_2ATP, adjusted to pH 7.2 with KOH; calculated chloride reversal potential is −90 mV) and #2 solution (in mM: 110 K-gluconate, 15 KCl, 2 $MgCl_2$, 10 HEPES, 10 EGTA, and 4 Na_2ATP, adjusted to pH 7.2 with KOH; calculated chloride reversal potential is −51 mV). These two solutions gave us similar results, and thus, we pooled the data. About one-fifth of our data were obtained using the #1 solution. The calculated liquid junction potentials, which we corrected for, were 16 mV (#1) and 5 mV (#2). The recordings were accepted for data analysis if the resting membrane potential of GFP-positive neurons was more negative than −53 mV. Neurons were labeled with a combination of 0.01% of Sulforhodamine B (Sigma) and 0.005% of Alexa Fluor 594 hydrazide (Invitrogen) in the patch solution. After penetration, neurons were briefly viewed with a long-path emission filter for GFP detection. In this configuration, a weak fluorescence signal from Sulforhodamine B was also visible. This made us confident that we were recording from GFP-positive cells, as penetration of the electrode added a slight orange color to the GFP cell. After the recordings, fluorescent images were acquired with a CCD camera (C2741; Hamamatsu Photonics, Hamamatsu, Japan) and a frame grabber (LG3; Scion, Frederick, MD). Identities of neuronal types were determined using anatomical features. All of the GFP-positive neurons recorded from were ipsilateral descending neurons. Motoneurons were identified by their torn axons at the lateral edge of the ventral spinal cord. In some experiments, a combination of 10 μM CNQX and 50 μM D-AP-5 (both from Tocris Cookson, Bristol, UK) was applied briefly (1–3 min) to the extracellular solution. Tetrodotoxin (TTX; 1 μM; Sigma) was also applied in some experiments. Latency of EPSPs was measured from the peak of the presynaptic spike to the onset of the EPSP.

In the main *alx*-expression domain at the stage we analyzed (52–62 h of development), intensely labeled cells tended to be located in the medial region. In the very early phase of our experiments, we recorded from these brightly labeled cells and learned that they were very often immature neurons. These cells did not show spiking activity during fictive locomotion, nor they did fire after direct current injection to the soma. We did not include these immature neurons in our data analysis. After this, we preferentially recorded from cells located more laterally. Paired recordings of *alx* neurons with VR or motoneurons showed that all *alx* neurons received rhythmic synaptic inputs when fictive swimming was occurring. This allowed us to estimate whether the stimulation elicited fictive locomotion and how long it lasted even when we only recorded from *alx* neurons. For this reason, we included single recordings ($n = 29$; the number includes the paired recordings with other interneurons; see below) in our data analysis for evaluating the spiking activity of *alx* cells during fictive swimming. A small fraction of our data included paired recordings of *alx* cells with neurons other than motoneurons. We included those recordings in our data analysis as single recordings. In this study, we recorded from 105 *alx* neurons, of which 63 were paired recordings with motoneurons, 13 were with VR, and 29 were single recordings.

We only analyzed episodes that lasted for >1 s (in most cases, the episode duration was longer than this). Episodes were generally picked at random, but typically the first trial after getting whole-cell was examined. When several episodes were elicited in the same cell, the spiking patterns were consistent. The dorsoventral position of the recorded neurons was examined by measuring the distance between the center of the recorded cell and the ventral boundary of the spinal cord.

Electroporation of rhodamine–dextran into single cells. Single cell labeling with rhodamine–dextran by electroporation was performed essentially as described by Bhatt et al. (2004). Procedures of sample preparation and bathing solution were identical to those for patch recordings (see above). Electrodes having a slightly wider tip diameter (10–20 MΩ in resistance) were filled with 4% tetramethylrhodamine-conjugated dextran (M.W., 3000; Invitrogen) in patch solution. After touching a GFP-labeled cell, voltage pulses were applied using an isolated pulse stimulator (model 2100; AM Systems, Carlsborg, WA). The stimulation parameters used were: 6–9 V for voltage pulse amplitudes, 3 s for train burst width with a 1 ms pulse duration and 9 ms interpulse intervals. After labeling, preparations were kept for 30 min in extracellular solution and then mounted in low-melting point agarose in the same solution.

Results

Distribution of *alx*-positive cells in the spinal cord

We first examined the developmental profile of *alx* expression in the spinal cord by *in situ* hybridization. Because there is a rostrocaudal developmental gradient in the spinal cord, especially at early stages, we focused on one region at midbody, from approximately segment 7–12 (the same midbody region was examined in all of our experiments).

Weak *alx* expression was first detected in a small number of cells at ~20 hpf (at 28.5°C; data not shown). At 24 hpf, clear *alx* expression was discernible in a small number of cells located in the ventral to intermediate region of the spinal cord (Fig. 1*A*,*B*). As development proceeded, the number of *alx*-expressing cells gradually increased, such that by 32 hpf (Fig. 1*C*,*D*) more *alx*-expressing cells were apparent (Fig. 1, compare *B*, *D*) (the average number of positive cells per hemisegment increased from 2.6 to 4.6 during this period). Postmitotic neurons are located only in

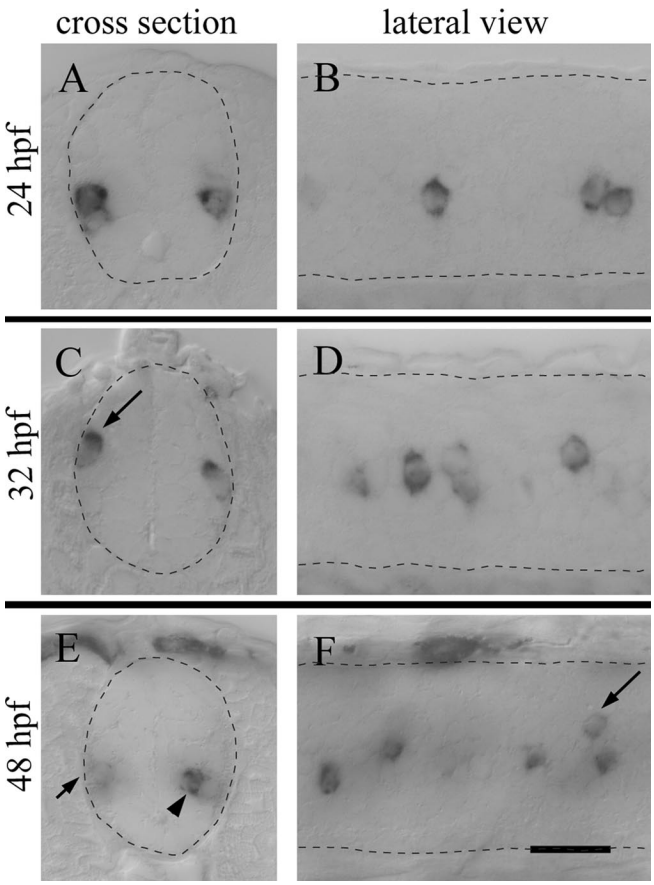

Figure 1. *alx* mRNA expression patterns in embryos. Spinal cords at three different stages (24, 32, and 48 hpf) were stained with *alx in situ* hybridization. The left panels show cross sections of the spinal cord, whereas the right panels show a lateral view. Dorsal is to the top. In the right panels, rostral is to the left (the same for all the subsequent figures). The long arrows in ***C*** and ***F*** indicate cells located in a more dorsal region of the spinal cord. The arrowhead in ***E*** indicates an intensely labeled cell that is located in the medial region. The short arrow in ***E*** shows a faintly labeled cell located in the lateral region. The dark spots located outside the spinal cord in ***E*** and ***F*** are from pigment cells, and they are not *in situ* hybridization signal. Scale bar, 20 μm.

the lateral region of the spinal cord at these early stages. Consistent with this, all of the *alx*-positive cells were located near the lateral margin (Fig. 1*A*, *C*). Figure 1, *E* and *F*, shows the expression pattern of *alx* in 48 hpf embryos. At this stage, *alx*-expressing cells were located not only in the margin but also in more medial regions (Fig. 1*E*, arrowhead). Medially located cells were likely to have formed between 32 and 48 hpf. The staining intensity of *alx*-expressing cells near the margin tended to be faint at 48 hpf (Fig. 1*E*, arrow). Because laterally located cells are likely to be the ones that formed at earlier stages, this suggests that *alx* expression was downregulating in the faintly labeled cells. The number of *alx*-positive cells slightly increased between 32 hpf (Fig. 1*D*) (4.6 per hemisegment on average) and 48 hpf (Fig. 1*F*) (5.8 per hemisegment on average). However, a more robust increase was observed in the number of cells that had expressed *alx* in their developmental history during this time period (see the following section). This suggests that some of the cells that had expressed *alx* did not have detectable levels of *alx* expression at 48 hpf.

It is worth noting that throughout development, the main *alx* expression domain was found within the ventral to intermediate region of the spinal cord, which covers ~25–50% of the bottom of the spinal cord. However, occasional *alx*-positive cells located in a more dorsal region were observed at later stages (Fig. 1*C*, *F*, arrows).

Visualization of *alx*-positive cells in living fish

To visualize *alx*-positive cells in living animals, we generated transgenic fish expressing GFP using the BAC homologous recombination technique (Fig. 2*A*) (Lee et al., 2001). Among the three transgenic fish lines generated, only the line having the highest expression was used for further analysis (called *alx*:GFP hereafter). Figure 2*B* shows the GFP expression pattern in a live *alx*:GFP embryo at 3 d postfertilization (dpf). In addition to expression in the spinal cord, GFP expression was also observed in the hindbrain and eye, consistent with the previous report that showed that *alx* was expressed in these regions (Barabino et al., 1997). We first examined whether *alx* expression was accurately recapitulated by GFP expression. Dual *in situ* hybridization of *alx* and *gfp* was performed in transgenic fish. As shown in Figure 2*C*, mRNA expression of *alx* and *gfp* completely overlapped. This therefore allowed us to examine the nature of *alx*-positive cells using the transgenic fish.

GFP expression patterns in the transgenic fish were generally similar to *alx* mRNA expression patterns. However, at later stages, GFP expression was discernible in more cells than *alx* mRNA. For example, the average number of GFP-positive cells per hemisegment at 48 hpf was 12.2, whereas that of *alx*-positive cells was 5.8. This is because the expression of *alx* mRNA is transient, but GFP expression is more stable. Thus, in transgenic fish, cells that had expressed *alx* at any given time point in their developmental history were labeled with GFP. In the rest of the text, these GFP-positive cells, which serve as records of *alx*-expression, are called *alx* cells or *alx* neurons. Figure 2, *D* and *E*, shows confocal stacked images from a lateral view and a cross section of a transgenic fish at 56 hpf (early 2 d). As expected, GFP-positive cells were predominantly located in the main *alx* expression domain. However, as seen with *alx* mRNA expression, GFP-positive cells that protruded into more dorsal regions were occasionally observed (Fig. 2*D*,*E*, long arrows). In the main *alx*-expression domain, lightly labeled cells tended to be located in more lateral regions (Fig. 2*E*, the cells marked by the short arrow and open arrowhead). We speculate that laterally located cells with light GFP labeling correspond to earlier differentiating neurons that had expressed *alx* early in their developmental history. Medially located cells with intense GFP labeling were likely to be later-born neurons (Fig. 2*E*, the cell marked by the closed arrowhead). GFP-positive cells that protruded in the dorsal region of the cord were always laterally located, near the margin (Fig. 2*E*, the cell marked by the long arrow).

alx cells are likely to derive from the p2 progenitor domain

In amniotes, Chx10-positive cells are derived from the p2 progenitor domain (Briscoe et al., 2000). In zebrafish, however, the developmental origin of *alx* cells has not been examined. Some of the *alx* cells were located much more dorsally than V2 neurons (neurons that derive from the p2 progenitor domain) would "normally" be located. These cells might not be specified in the p2 progenitor domain. If so, the developmental scheme of *alx* cells in zebrafish would differ from Chx10 cells in amniotes. To clarify this point, we examined whether GFP-positive cells had the characteristics of V2 neurons by performing immunostaining at 32 hpf, because such dorsally located cells were apparent by this time (Fig. 1*C*, arrow).

In amniotes, Nkx6.1 demarcates the dorsal boundary of the p2

progenitor domain in the ventricular zone. Nkx6.1 is also expressed in postmitotic neurons (Sander et al., 2000). Therefore, if GFP-positive cells were also positive for Nkx6.1, that would indicate a p2 origin for GFP-positive cells. As shown in Figure 3*A*, all the GFP-positive cells including ones located in the dorsal region (arrow) were positive for Nkx6.1. This suggests that dorsally located GFP-positive cells were born in the p2 progenitor domain and then migrated dorsally. The Nkx6.1 staining also showed that most of the other GFP-positive cells (arrowheads) were shifted slightly dorsally from the dorsal edge of the main Nkx6.1 expression domain. This suggests that a dorsalward migration of *alx*-positive cells is a general trend, at least up to 32 hpf. We also performed Lhx3 antibody staining. Lhx3, in amniotes, has been shown to mark both V2 neurons and motoneurons (Ericson et al., 1997; Sharma et al., 1998; Thaler et al., 1999). As shown in Figure 3*B*, all GFP-positive cells were also positive for Lhx3.

We also investigated the dorsoventral relationship between *alx* cells and either V1 neurons or motoneurons. En1 and Isl1 were used as markers for V1 neurons and motoneurons, respectively (Ericson et al., 1997; Briscoe et al., 2000). As shown Figure 3*C*, the location of En1-positive cells was, on average, more dorsal than the location of *alx*:GFP-positive cells. However, some ventrally located En1-positive cells were more ventrally located than dorsally located *alx*:GFP-positive cells. Given that *alx* cells show a dorsalward migration at this stage, it is likely that En1 neurons also have a dorsalward migration. Regardless, our data are consistent with the notion that En1-positive cells derive from a more dorsal region (p1 progenitor domain) than *alx* cells (p2 progenitor domain). Figure 3D shows immunostaining of Isl1 in a transgenic embryo. As expected, the average location of *alx*:GFP-positive cells was more dorsal than the dorsal edge of the Isl1-positive motoneuron domain (Fig. 3*D*) (note that Isl1 is expressed in more dorsal cells that are not motoneurons). As with En1, intermingling did occur at each cell level

In summary, our results suggest that all *alx* cells derive from the p2 progenitor domain. (This does not mean that *alx* cells represent the entire population of V2 neurons; in amniotes, Chx10-positive cells are known to mark only a subset of V2 neurons.) The presence of dorsal *alx* cells is attributable to their dorsalward migration at early stages. Also, the topographic relationship among V1, V2, and motor neurons is maintained, although intermingling does occur at the borders of each domain.

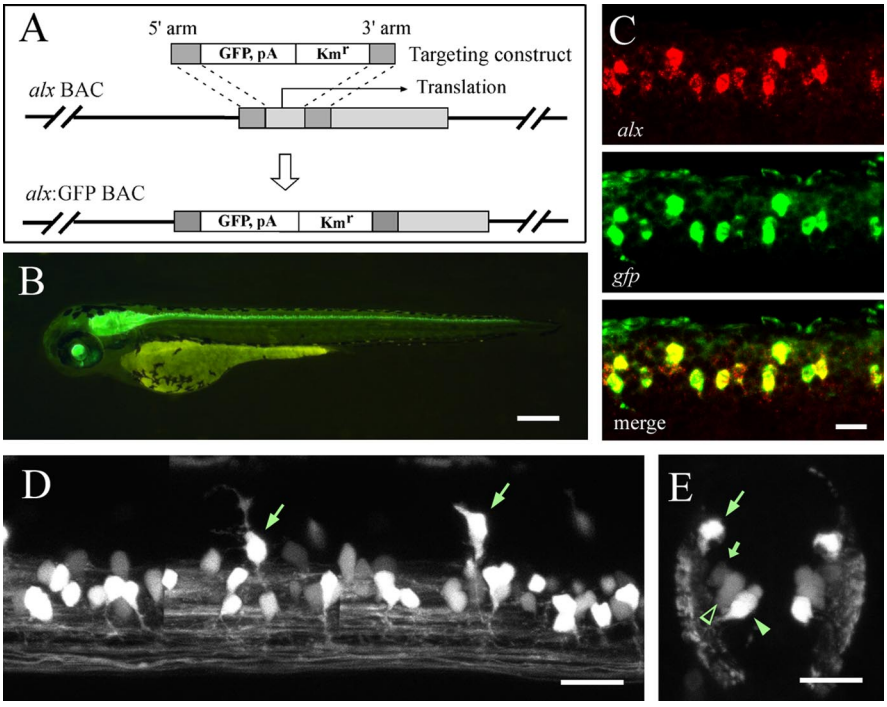

Figure 2. The *alx*:GFP BAC construct and an *alx*:GFP transgenic fish. ***A***, Construction of the *alx*:GFP BAC. Template DNA was PCR-amplified from a plasmid containing GFP, BGH poly(A) (pA), and Km^r. Each primer contained 50 bp of the *alx*-derived sequences that served as homology arms for homologous recombination (top drawing). The *alx* BAC contained 120 kb upstream and 20 kb downstream of the gene. After homologous recombination, GFP was inserted between the transcription start site and the translation start site (middle drawing). The bottom drawing shows the structure of the *alx*:GFP BAC used for generating transgenic fish. ***B***, An *alx*:GFP transgenic fish at 3 dpf. ***C***, Double *in situ* hybridization of *alx* and *gfp* in an *alx*:GFP transgenic fish at 32 hpf. The top panel shows the staining of *alx* mRNA, whereas the middle panel shows the staining of *gfp* mRNA. The bottom panel shows the merged image, in which *gfp* and *alx* staining completely overlapped. ***D***, Confocal image of an *alx*:GFP transgenic fish at 56 hpf. Several optical sections were stacked, and montages were made using the stacked images. The arrows point to cells protruding into the dorsal region. ***E***, Cross section of an *alx*:GFP transgenic fish at 52 hpf observed by confocal microscopy. Several optical sections were stacked (thickness of the total optical section, ~18 μm). The long arrow shows a cell located in a more dorsal region. The short arrow indicates a cell located near the dorsal edge of the main *alx* expression domain. The open arrowhead indicates a cell located in the middle or ventral and lateral region of the main *alx* expression domain. The closed arrowhead indicates a cell located in the medial region. Scale bars: ***C–E***, 20 μm; ***B***, 250 μm.

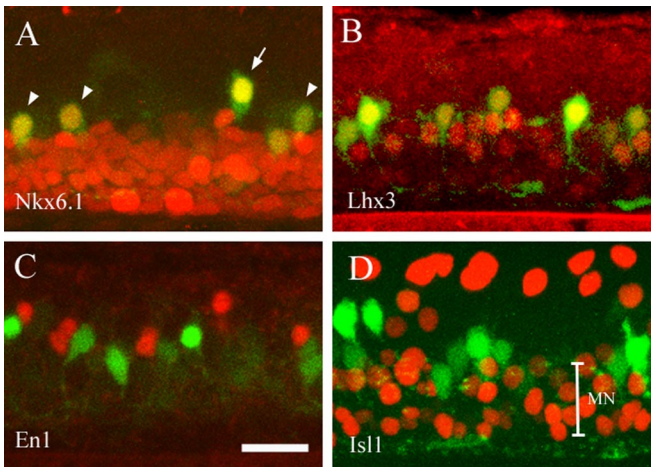

Figure 3. *alx* cells have properties of V2 neurons as determined by immunohistochemical analysis in *alx*:GFP transgenic fish at 32 hpf. ***A***, Lateral view of immunostaining with Nkx6.1. The green signal is from GFP, whereas the red signal is from Nkx6.1 immunohistochemistry. All of the GFP-positive cells are Nkx6.1 positive. In addition to the dorsal cell marked by the arrow, most of the other GFP-positive cells (arrowheads) are also slightly shifted dorsally from the dorsal edge of the main Nkx6.1 expression domain. ***B***, All of the GFP-positive cells are also positive for Lhx3. ***C***, GFP and En1 expressions are mutually exclusive. ***D***, GFP and Isl1 expressions are mutually exclusive. MN, Motoneuron domain. Scale bar, 20 μm.

Early born *alx* cells are more dorsally located than later-born ones

We then examined the topographic relationship between early born *alx* neurons and later-born ones. For this purpose, we generated another transgenic fish expressing photoconvertible fluo-

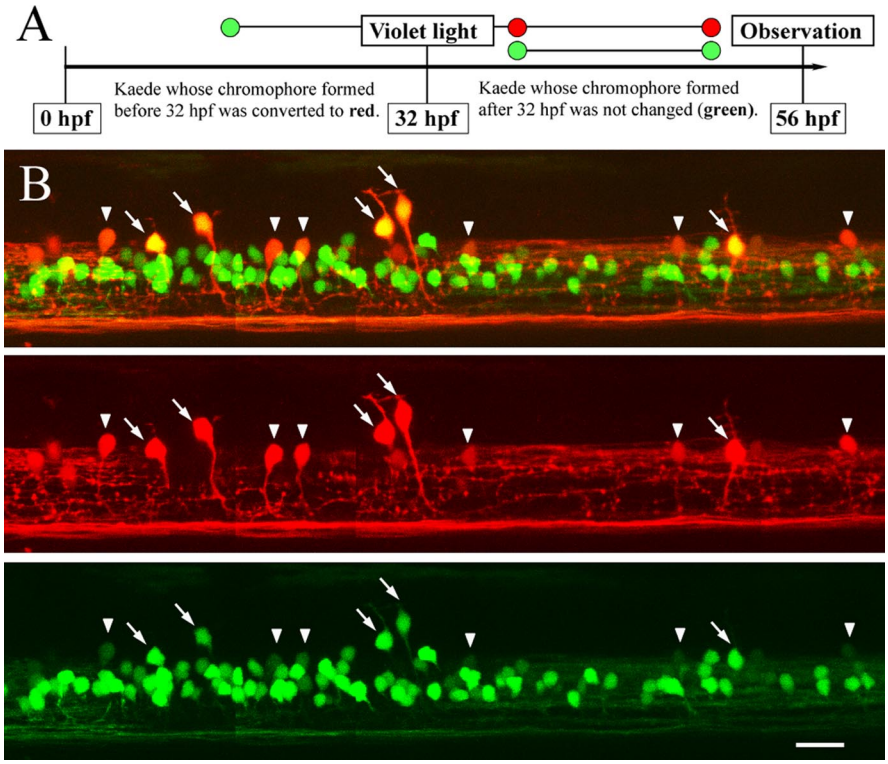

Figure 4. *alx*:Kaede transgenic fish reveal that early born *alx* cells are located in a more dorsal region. ***A***, Schematic diagram of the Kaede photo-conversion experiment. ***B***, A representative example of the Kaede photo-conversion experiment. The top panel shows a merged image of the green and red channels. The middle panel shows an image of the red channel. The bottom panel shows an image of the green channel. Several optical sections were stacked, and montages were made using the stacked images. The arrows indicate cells that have both red and green fluorescence. The arrowheads indicate cells that have red fluorescence with a marginal level of green fluorescence. All of the cells having a red color (arrows and arrowheads) are located in a more dorsal region. Scale bar, 20 μm.

rescent protein, Kaede (Ando et al., 2002), in *alx* cells. The experimental design was as follows: transgenic embryos were exposed to violet light at a certain developmental time point, so that virtually all the Kaede fluorescence at that time was converted from green to red. Then, the animals were allowed to grow until the time of the observation. Because fluorescent Kaede protein expressed after violet light illumination will show its original fluorescence (green), the presence of red color in a cell indicates that it expressed Kaede before illumination, whereas a cell having only green color means that Kaede protein was generated after illumination. Thus, cells of the former type could be judged as earlier differentiating neurons, whereas cells of the latter type were likely to be later forming neurons.

Violet light was applied at 32 hpf, and observations were made at 56 hpf (Fig. 4*A*). Figure 4*B* shows that virtually all the cells having a red color were located in a relatively dorsal region (arrows and arrowheads). This finding corroborated our previous results. Another important finding was that pure green cells were all located within the main *alx*-expression domain. This indicates that later-differentiating neurons did not show a dorsalward migration. Thus, we concluded that dorsally located cells are predominantly earlier-born neurons, whereas ventrally located cells are predominantly later-born neurons.

Examination of the confocal optical sections showed that cells having any red color were always located near the lateral region of the spinal cord. This is consistent with the notion that the earlier forming neurons tend to be located near the surface region of the spinal cord. Green cells tended to be located in the medial region, although more laterally located cells were also observed. It is likely that the green medially located cells form later than the green laterally located cells. It is also worth noting that very dorsally located cells tended to have both red and green color (cells having both colors are marked by arrows). This suggests that these cells express *kaede* mRNA for a longer period.

Morphology of *alx* neurons

In the *alx*:GFP or *alx*:Kaede transgenic fish, many cells were fluorescent, making it difficult to follow the dendritic and axonal morphologies of individual cells. To obtain isolated labeling in transgenic fish for morphological analysis, we used the Cre/loxP recombination system (Gu et al., 1994). Transgenic fish were made using the DNA construct shown in Figure 5*A*. In this construct, DsRed is sandwiched by two loxP sites. The resulting transgenic fish, *alx*:loxPDsRed-GFP, expressed DsRed in *alx* cells. By stochastically expressing Cre protein with a transient expression system in the stable *alx* transgenic fish, we could obtain fish in which a small, random subset of *alx* cells expressed GFP instead of DsRed, as Cre-mediated recombination flipped DsRed out. An example of this is shown Figure 5*A*. We examined a large number of GFP-positive cells, and all the cases in which axonal trajectories could be followed ($n > 60$) had the following common features: a primary axon that first extends ventrally, turns caudally in ventral spinal cord, and then descends on the ipsilateral side of the spinal cord in the marginal zone lateral to motoneurons, moving more dorsally as it descends (Fig. 5*A*, circle and asterisk). Ipsilateral descending neurons having similar morphological features have been observed previously in zebrafish and named circumferential ipsilateral descending (CiD) neurons or ventral longitudinal descending neurons (Bernhardt et al., 1990; Kuwada et al., 1990; Hale et al., 2001). However, because there is some confusion regarding the usage of these terms (Higashijima et al., 2004c), we primarily use the term *alx* cells to describe GFP-positive cells for the rest of the text.

The Cre/loxP recombination system was useful for examining the axonal trajectories of a large number of neurons with relative ease. Dendritic morphologies could also, to some extent, be revealed (Fig. 5*A*, the cell marked by an asterisk). However, a more careful analysis was often difficult, because in many cases, two cells located side by side were labeled (Fig. 5*A*, the cell marked by a circle). To obtain more isolated labeling, we filled individual GFP-positive cells with rhodamine–dextran dye by electroporation (Fig. 5*B*) (Bhatt et al., 2004). Electrophysiological recordings demonstrated that medially located cells (such as the cell marked by the closed arrowhead in Fig. 2*E*) were often immature, as indicated by their failure to spike after direct current injection (see Materials and Methods). Thus, we preferentially electroporated neurons located in a more lateral region of the spinal cord. We examined 30 neurons at 56–62 hpf. The dendritic morphology of *alx* cells was not completely homogeneous. Some were

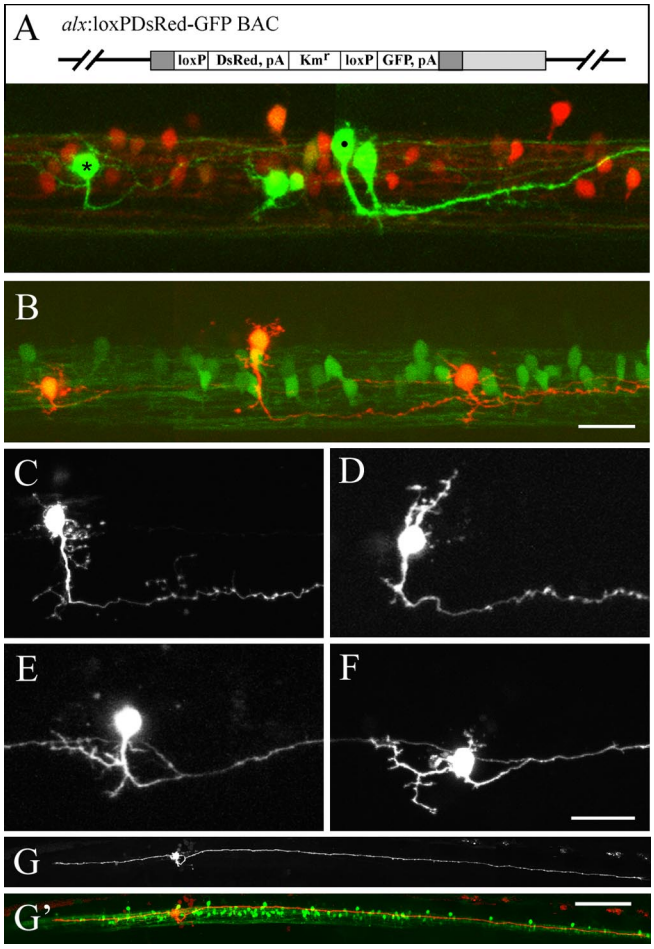

Figure 5. Single cell morphology of *alx* neurons. ***A***, The schematic (top) shows the structure of the construct for generating *alx*:loxPDsRed-GFP transgenic fish. The picture panel shows a confocal image of a 48 hpf *alx*:loxPDsRed-GFP transgenic fish injected with a Cre-containing plasmid. pA, Poly(A). ***B***, Lateral view of an *alx*:GFP transgenic fish in which three GFP-positive cells were loaded with rhodamine–dextran by electroporation. ***C–G′***, Single cell morphology revealed by rhodamine–dextran labeling. The fish were at 58–62 hpf. In ***G***, the entire morphology of a single *alx* neuron is shown. The descending main axon is much longer than the ascending branch. ***G′***, The image of GFP is also shown. The main descending axon runs near the dorsal edge of the main *alx* expression domain. The ascending axon runs in a slightly more ventral region. Scale bars: (in ***B***, ***F***) ***A–F***, 20 μm; (in ***G′***) ***G***, ***G′***, 100 μm.

unipolar with extensive dendrites emerging from the main axonal process (Fig. 5*E*), whereas in others, prominent dendrites came directly off the soma (Fig. 5*D*,*F*). In some cells, short dendrites came off both the soma and primary axonal process (Fig. 5*C*). There also appeared to be a difference in the dendritic morphology along the dorsoventral axis. Cells having dorsally extending dendrites were more often found in a relatively dorsal region, whereas cells having extensive ventral dendrites were more often found in a relatively ventral region. Single cell labeling also revealed that a significant fraction of *alx* cells had a rostrally extending axonal branch that arose from the proximal portion of the descending axon (Fig. 5*E–G′*). Cells having the rostrally extending secondary axon were more often found in the main *alx* domain, whereas dorsally protruding cells rarely had secondary axons. The rostrally extending axonal branch was short, spanning only one to four segments, whereas the caudally extending main axons tended to be longer (Fig. 5*G*,*G′*). We measured the length of the main axon in 10 cells and the average was 801 μm (SD, 96 μm), which approximately corresponds to 10–11 segments.

The vast majority, but not all, of ipsilateral descending neurons are *alx* cells

Our data so far demonstrate that all *alx* cells are ipsilateral descending neurons. One important question that remained was whether *alx* cells accounted for all the ipsilateral descending neurons. To address this question, we labeled ipsilateral descending neurons with methods that were independent of *alx* expression and asked whether the labeled cells were *alx* cells. We first used backfilling. Backfill labeling in previous studies (Bernhardt et al., 1990; Hale et al., 2001) has identified ipsilateral descending neurons called CiDs. We performed backfilling with Texas Red in *alx*:GFP embryos at 50–54 hpf and observed the backfilled fish at 58–62 hpf. We obtained 25 cells (in 13 fish) that were morphologically identified as CiD interneurons. A representative example is shown in Figure 6*A*, in which all the labeled CiD cells were GFP positive. It should be noted that in these experiments, only a small number of neurons were purposely labeled with a small injection. This was necessary for the morphological identification of labeled neurons. A larger injection resulted in too many labeled axons, making it difficult to follow the axonal trajectory of the individual neurons. We also performed backfilling experiments at 4–5 dpf, the same stage when the previous backfilling experiments were performed. All but one ($n = 15$) of the CiD cells had GFP labeling (data not shown). In the one negative cell, GFP expression by this stage might have been downregulated below detection. In summary, the vast majority, possibly all, of the CiD cells that were identifiable by backfilling were among the *alx* cell population.

Because there was a concern that not all the ipsilateral descending neurons were identifiable by backfilling, we used an additional labeling approach. A pan-neuronal promoter (goldfish neural tubulin promoter) (Hieber et al., 1998) was used to drive transient, stochastic expression of mRFP (Campbell et al., 2002) in many different classes of spinal neurons. We obtained 13 cells (in 13 fish) that were morphologically identified as ipsilateral descending interneurons at 48–60 hpf. We found that the vast majority (11 of 13) of those cells had GFP labeling (two examples are shown in Fig. 6*B*,*C*), consistent with the results of our backfilling. In two cases, however, the morphologically identified ipsilateral descending neurons did not have a detectable level of GFP fluorescence (Fig. 6*D*). The morphology of these two negative cells was similar to *alx* cells. The only noticeable difference was in the axonal trajectory along dorsoventral axis: axons of *alx* neurons gradually migrate dorsally as they descend along the cord in all cases (Figs. 5*A*,*B*, 6*A–C*), whereas it appeared that the axon of the *alx*-negative cell continued to run in the more ventral region of the spinal cord (Fig. 6*D*, arrow) (the axon of the other *alx*-negative cell also ran ventrally).

In summary, the results of backfilling and stochastic labeling showed that the vast majority (100% for backfilling; 11 of 13 for stochastic labeling) of ipsilateral descending interneurons were among the *alx* cell population, although minor fraction of *alx*-negative ones did exist.

alx neurons are likely to be glutamatergic

We examined the neurotransmitter phenotype of *alx*-positive neurons by double *in situ* hybridization with *alx* and with genes whose expression patterns are tightly related to a particular neurotransmitter. Double staining with *vglut2* (a mixture of *vglut2a* and *vglut2b*) (Higashijima et al., 2004b), a marker for glutamatergic neurons, indicated that the vast majority of the *alx*-positive cells were positive for *vglut2*. A representative example is shown in Figure 7*A*, in which virtually all of the *alx*-positive cells were

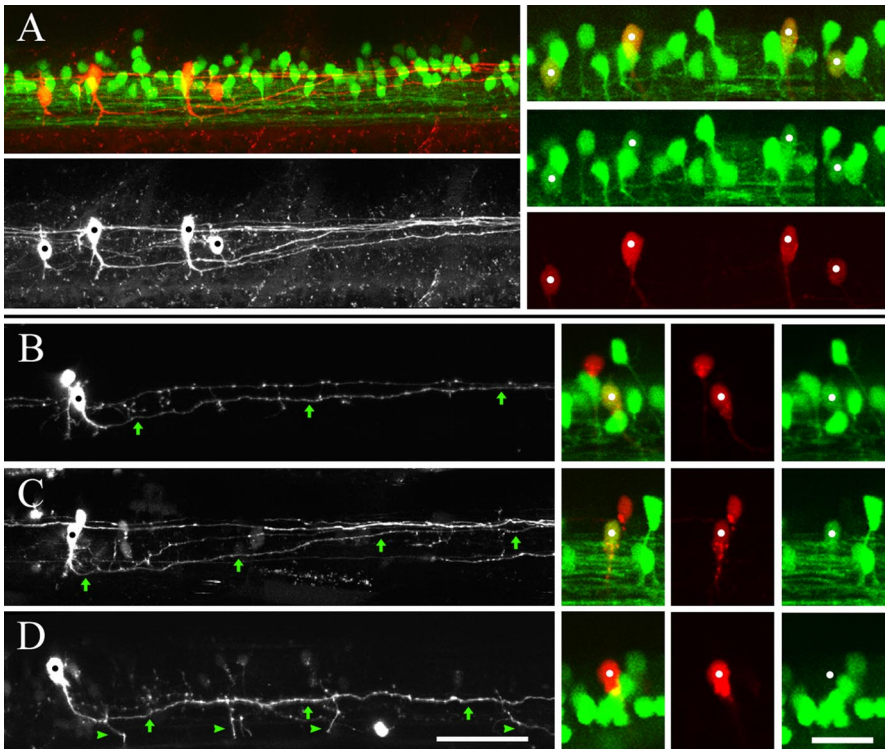

Figure 6. The vast majority of ipsilateral descending neurons are *alx* neurons. ***A***, Texas Red–dextran was pressure injected into the caudal spinal cord of an *alx*:GFP transgenic embryo. The left top panel shows a lateral confocal image of a backfilled embryo at 60 hpf. The red signal is from Texas Red, whereas the green signal is from GFP. The left bottom panel shows the Texas Red image only. Four ipsilateral descending neurons (dots) could be identified. The three right panels show magnified images of the four cells (merged view, GFP signal, and Texas Red signal). All of the four cells (dots) are positive for GFP. ***B–D***, Ipsilateral descending neurons labeled by stochastic expression of mRFP (dots). The left panels show images of mRFP. The arrows show axons of the ipsilateral descending neurons. The right three panels for each figure (***B–D***) show magnified images of the cell (merged view, mRFP signal, and GFP signal). ***B***, ***C***, Representative examples of ipsilateral descending neurons that are positive for GFP. Majority of mRFP-labeled ipsilateral descending neurons (11 of 13) had GFP labeling. ***D***, Minor fraction of ipsilateral descending neurons (2 of 13) did not have a detectable level of GFP. An example is shown. The arrowheads indicate signals that come from axonal collaterals of an mRFP-labeled reticulospinal axon. Scale bars: (in ***D***, left) ***A–D***, left, 50 μm; (in ***D***, right) ***A–D***, right, 20 μm.

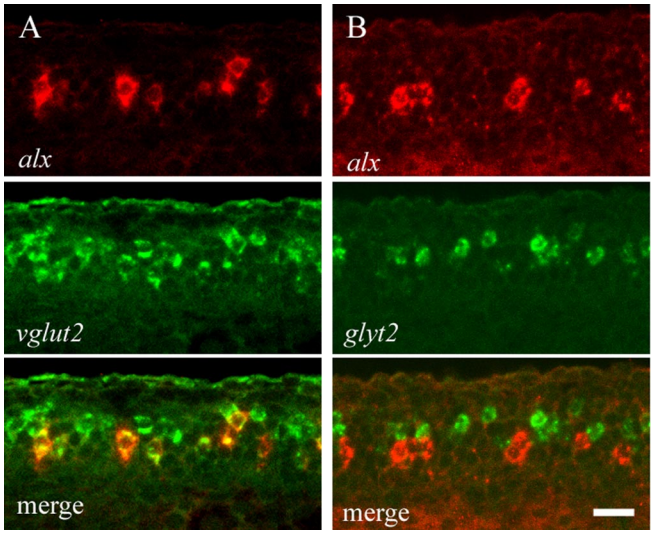

Figure 7. *alx*-positive neurons are likely to be glutamatergic. Images were taken from 32 hpf embryos. ***A***, Dual *in situ* hybridization of *alx* and *vglut2*. All of the *alx*-positive cells are *vglut2* positive. ***B***, Dual *in situ* hybridization of *alx* and *glyt2*. None of *alx*-positive cells are positive for *glyt2*. Scale bar, 20 μm.

positive for *vglut2*. These results strongly suggest that *alx* neurons are glutamatergic neurons. Occasionally, we observed *alx*-positive cells that were not accompanied by a detectable level of *vglut2* staining. We speculate that *alx* expression precedes *vglut2* expression in the history of the cell and that those apparent *vglut2*-negative *alx* cells would start expressing *vglut2* afterward. Consistent with the idea that *alx* cells are glutamatergic, double staining of *alx* and *glyt2* (Higashijima et al., 2004b), a marker for glycinergic neurons, showed that no *alx*-positive cells were ever positive for *glyt2* (Fig. 7*B*). We also examined markers for GABAergic neurons. For this purpose, we cloned a *viaat* gene from zebrafish (see Materials and Methods). The VIAAT protein is responsible for loading GABA and glycine into the synaptic vesicles of inhibitory neurons and is known to be expressed in GABAergic and glycinergic neurons (Sagne et al., 1997). Double *in situ* hybridization of *alx* and *viaat* showed that none of the *alx*-positive cells were positive for *viaat* (data not shown). These results support the view that *alx* cells are glutamatergic excitatory neurons.

Electrophysiology of *alx* neurons

Previous calcium imaging studies in larval zebrafish have shown that some CiD cells are active during escape behaviors (Ritter et al., 2001). Because the CiD cells identified by backfilling were among the *alx* cell population, it is likely that some of the *alx* cells are active during escapes. In addition, studies in frog tadpoles and adult lampreys have shown that ipsilateral descending neurons are the main source of on-cycle excitation during swimming (Dale and Roberts, 1985; Buchanan and Grillner, 1987; Roberts et al., 1998; Buchanan, 2001). Because *alx* neurons are ipsilateral descending excitatory neurons, we would expect that they perform a similar role during swimming in zebrafish. To investigate whether *alx* cells were indeed active during escapes and/or swimming and to investigate firing patterns of the *alx* cells during these behaviors, we performed electrophysiological recordings from *alx* neurons during fictive locomotion. In many of our experiments, we also monitored motor activity by simultaneously recording from peripheral motor nerves (VR) (Fig. 8) or a motoneuron (Fig. 9). All of the electrophysiological recordings were made using hatchling embryos at 52–62 hpf. At this stage, the embryo is generally sedentary, but sudden stimulation can initiate swimming that lasts for several seconds. With a strong stimulus to the head, embryos often performed a robust escape behavior: a very fast forceful C-shaped bend to the opposite side of the stimulus. Then, the escape was followed by a long bout of swimming. In our electrophysiological recordings, an electrical stimulation was applied near the head (either ipsilaterally or contralaterally) to elicit fictive locomotion. Motor activity that corresponded to swimming was reliably elicited, as demonstrated by rhythmic ventral root activity (Fig. 8), or by rhythmic spiking activity in motoneurons

(Fig. 9*Ab*,*Bb*,*Db*). As described below, fictive motor activity corresponding to escapes could also be elicited.

During fictive locomotion elicited by electrical stimulation, all of the *alx* cells we examined ($n = 105$) showed rhythmic oscillations in membrane potential (Figs. 8, 9). Many of the *alx* cells (87 of 105) also showed spiking activity in at least one of these bouts of locomotion. The spiking patterns observed differed from cell to cell but could be approximately categorized into two groups. In one group, spiking activity only occurred during the initial part of the episode (Figs. 8*A*,*B*, 9*A–C*). When the stimulus was applied to the contralateral side, these *alx* cells typically showed spiking activity with very short latency to the stimulus (<10 ms) (Fig. 9*Ac*,*Bc*). The spiking activity likely corresponded to escape behavior. Consistent with this, multiple spikes in motoneurons (indicative of strong movement) were often observed (Fig. 9*Ac*,*Bc*). The timing of spikes in *alx* cells mostly coincided with or slightly preceded motoneuron spikes (Fig. 9*Bc*,*Ac*, respectively). In addition to the spikes associated with the escape, some of the *alx* neurons of this class also fired afterward for several cycles (Figs. 8*A*, 9*Bc*). We presume that the activity that occurred only in the initial part of the episode corresponded to faster swimming that typically follows an escape. Consistent with this idea, the cycle period of ventral root activity or motoneuron activity in the earlier part of the swimming episode was often shorter than the later part (Figs. 8*A*,*B*, 9*Ab*). In some cases, larger signals in the ventral root recording were observed during the initial part of the swimming episode, further supporting the idea that more motor units were active. In summary, *alx* cells of this class fired during escape behaviors, and some of them also fired during faster swimming. Therefore, we call this class of *alx* cells the "strong movement" type or strong class. The other class of *alx* cells showed spiking activity for almost the entire duration of the swimming episode (Figs. 8*C*, 9*Db*). Spiking activity in these *alx* cells occurred in phase with nearby ventral root activity or motoneuron activity (Fig. 9*Dc*). We call this class of *alx* cells the "weak movement" type or weak class to highlight their involvement in slow swimming. It should be noted, however, that many of the *alx* cells of this class (~80%) also showed spiking activity during the initial part of the episode (Fig. 9*Db*), and thus, activity of these neurons was not specific to weak movement. A fraction of the cells (~20%) did not fire during the initial part and then started firing consistently for the rest of the swimming episode (Fig. 8*C*). Thus, there were neurons whose activity was specific to slower movement.

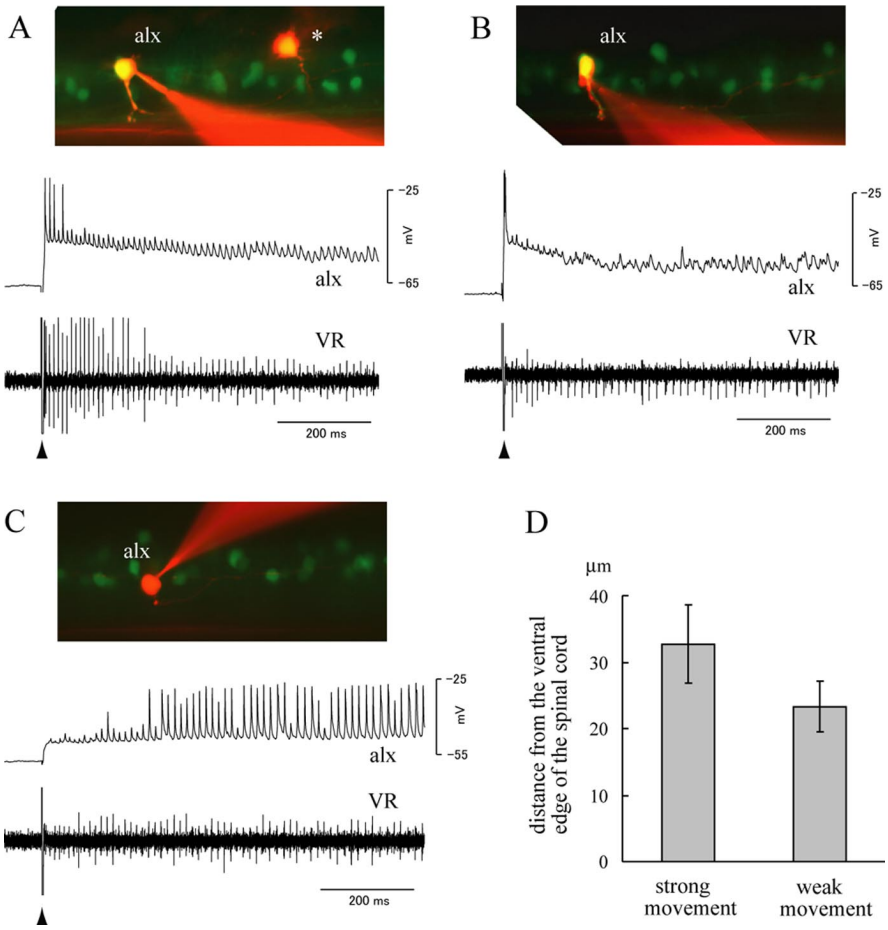

Figure 8. Activity of the *alx* neurons during fictive locomotion. ***A–C***, Simultaneous recordings between *alx* neurons and a VR. The experiments were performed in the *alx*:GFP embryos at 52–62 hpf (the same for the subsequent figures). Patch electrodes were targeted to GFP-positive cells to record from *alx* neurons. Fictive locomotion was elicited by applying a brief electrical stimulation near the ear at the time point indicated by the arrowhead. In the experiments shown in ***A–C***, the stimulation was applied on the contralateral side. The top of each panel shows the image after electrophysiological recording, whereas the middle and bottom show the whole-cell recordings from the *alx* neuron and the ventral root recording, respectively. The asterisk in ***A*** shows a cell that was labeled on an earlier attempt. The cell is unrelated to the recording shown in ***A***. ***D***, A graph that shows the average dorsoventral location of strong-movement-type *alx* neurons and weak-movement-type *alx* neurons. The dorsoventral location of the recorded cell was quantified by measuring the distance of the cell from the ventral edge of the spinal cord. Thirty cells for each class were examined, and the average distance is shown with the SD (error bars).

There was a correlation between the firing patterns of the *alx* cells and the dorsoventral position of the cells. Among the *alx* cells located in the main *alx* domain, dorsally located cells tended to fall into the strong movement type (Fig. 8*A*,*B*), whereas those located ventrally tended to fall into the weak movement type. Notably, all of the cells that protruded dorsally from the main *alx* domain fell into the strong movement type. An example of such a dorsally located cell is shown in Figure 9*Aa*. Quantitative analysis measuring the distance of each cell from the ventral edge of the spinal cord also supported this correlation (Fig. 8*D*) ($p < 0.001$, *t* test). Given that dorsally located cells were earlier differentiating neurons, we concluded that among *alx* cells, those that differentiate earlier tend to be involved in stronger movements, whereas those that differentiate later tend to be involved in weak movement. It should be noted that although the vast majority of *alx* cells were easily classified into each group, a minor fraction of them (~5%) exhibited an intermediate character. For example, some neurons fired mainly during the initial phase, and for the rest of the swimming episode, they fired sporadically (data not shown). Also, some of the cells of strong movement type only fired during escapes (Fig. 8*B*), whereas others fired in the subsequent faster swimming (Fig. 8*A*). Finally, some of the weak movement cells often skipped cycles. Therefore, although *alx* cells could be approximately categorized into two groups, the

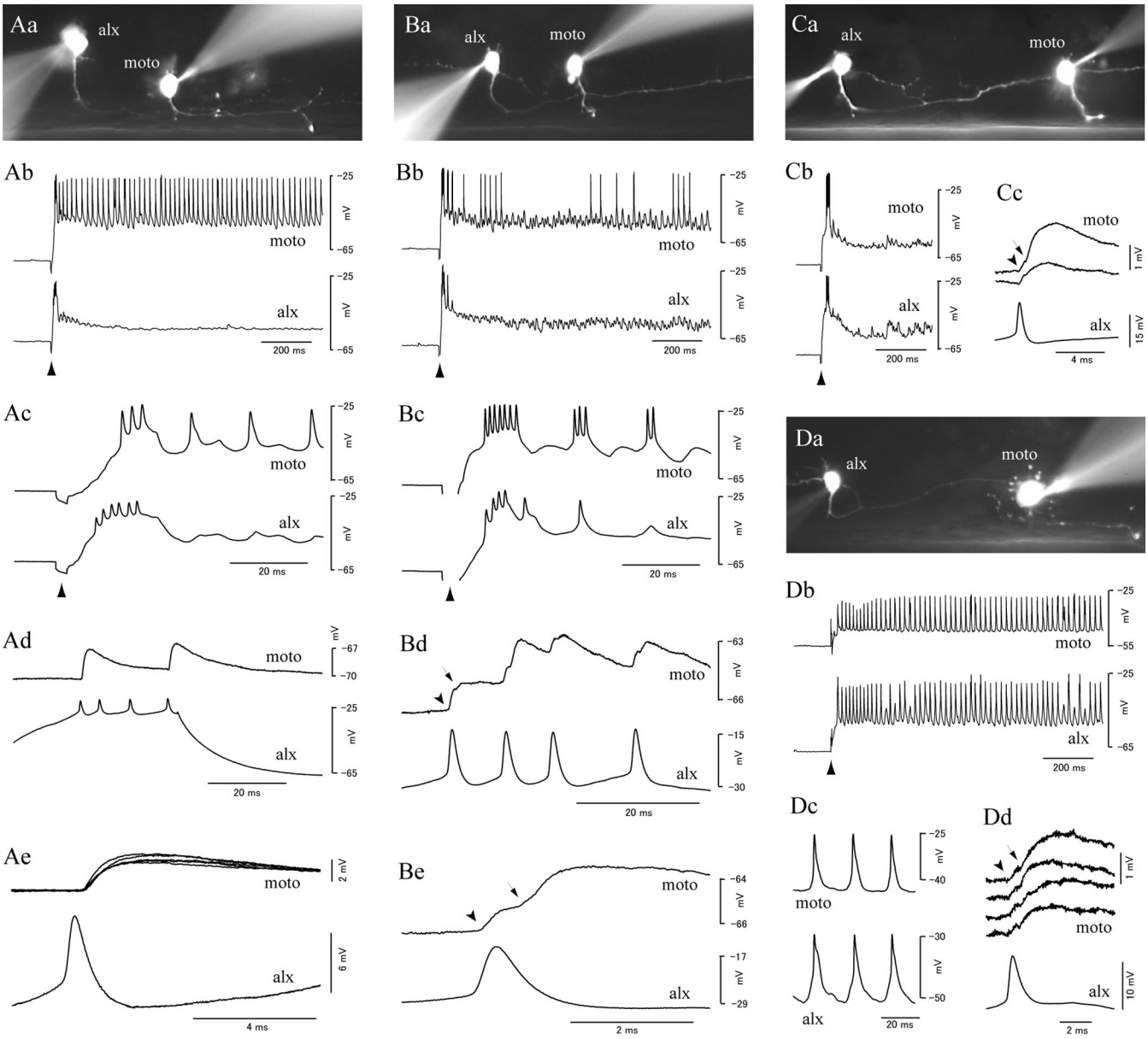

Figure 9. Paired recordings show that *alx* neurons make monosynaptic connections onto motoneurons. The pictures (***Aa***, ***Ba***, ***Ca***, ***Da***) show images of the recorded cells. Motoneurons (moto) were identified by their torn axons at the lateral edge of the ventral spinal cord. Fictive locomotion was elicited by applying a brief electrical stimulation near the ear at the time point indicated by the arrowheads (***Ab***, ***Ac***, ***Bb***, ***Bc***, ***Cb***, ***Db***). In the experiments shown in ***A*** and ***B***, the stimulation was applied on the contralateral side, whereas in the experiments shown in ***C*** and ***D***, it was applied on the ipsilateral side. ***Aa–Ae***, A paired recording between a strong-movement-type *alx* neuron and a motoneuron. ***Ab***, ***Ac***, Activity of the *alx* neuron and the motoneuron during fictive locomotion. ***Ac*** shows a close-up view near the onset of locomotion. ***Ad***, The current-evoked spikes (the first and the fourth spikes) in the *alx* neuron lead to EPSPs in the motoneuron. Synaptic failures occurred for the second and third spikes. ***Ae***, Five superimposed traces of EPSPs in the motoneuron. The traces show short, constant latency EPSPs. Only one spike in the *alx* neuron is shown for simplicity. Traces of EPSPs in the motoneuron are aligned with the peak of the spikes of the *alx* neuron. ***Ba–Be***, A paired recording between a strong-movement-type *alx* neuron and a motoneuron. ***Bb***, ***Bc***, Activity of the *alx* neuron and the motoneuron during fictive locomotion. ***Bc*** shows a close-up view near the onset of locomotion. ***Bd***, Four current-evoked spikes in the *alx* neuron lead to EPSPs in the motoneuron. All four EPSPs show two components as indicated by the arrowhead and arrow in the first EPSP. ***Be***, A close-up view of the dual-component EPSP. The first component EPSP (electrical; arrowhead) occurred earlier than the peak of the presynaptic spike, whereas the second component EPSP (chemical; arrow) occurred with a very short latency. ***Ca–Cc***, A paired recording between a strong-movement-type *alx* neuron and a primary motoneuron. ***Cb***, Activity of the *alx* neuron and the motoneuron during fictive locomotion. The spiking activity in the motoneuron is only observed during the initial phase of the locomotor episode. ***Cc***, Current-evoked spikes in the *alx* neuron lead to EPSPs in the motoneuron. Two traces are shown. Both traces show dual-component EPSPs (arrowhead and arrow). ***Da–Dd***, A paired recording between a weak-movement-type *alx* neuron and a motoneuron. ***Db***, Activity of the *alx* neuron and the motoneuron during fictive locomotion. ***Dc***, A close-up view in the middle of swimming. Three cycles of swimming are shown. ***Dd***, Current-evoked spikes in the *alx* neuron lead to EPSPs in the motoneuron. Four traces are shown. All of the traces show dual component EPSPs (arrowhead and arrow).

boundary between these two was not always completely clear, and there might in fact be a continuum.

A minor fraction of *alx* cells (18 of 105) did not fire during our recordings. All of these cells were located relatively dorsally. We presume that these cells belonged to the strong movement type and that fictive movements strong enough to make them fire were not elicited in these trials. Consistent with the idea, in experiments that were dedicated to eliciting escape behaviors by testing several stimulation strengths, all ($n = 13$) of the dorsally located cells except for one showed spiking activity associated with escapes. Thus, the vast majority, and possibly all, *alx* cells are likely to be involved in locomotor behavior. Among the 105 *alx*

neurons that we recorded from in this study, 60 neurons fell into the strong movement class (this number includes the 18 neurons that did not fire during fictive locomotion), and 45 neurons fell into the weak movement class.

The most likely role of *alx* neurons is to provide excitation onto motoneurons during both escapes and swimming. Thus, we examined possible synaptic connections between *alx* neurons and motoneurons using paired recordings. We will first describe synaptic connections between strong movement type *alx* neurons and motoneurons. Chemical connections were found between 22 of 47 pairs (this number includes mixed synapses; see below). Figure 9, *Ad* and *Ae*, shows a representative example. In each case, firing the *alx* neuron with somatic current injection produced short latency depolarizing PSPs in the motoneurons. The synaptic connections in some of the pairs were not reliable, meaning synaptic failures often occurred (Table 1), as demonstrated by the second and third spikes of the *alx* neuron in Figure 9*Ad*. However, whenever the PSPs were observed, they occurred with the very short latencies (ranging between 0.3 and 0.7 ms) (Table 1). The latencies were also very constant (<0.15 ms of SD for each pair) (Table 1). To further confirm that the connections were monosynaptic, paired recordings were performed in a high-divalent cation solution. A high-divalent cation concentration raises spike threshold (Frankenhaeuser and Hodgkin, 1957) and thereby reduces conduction in polysynaptic pathways. The results showed that the connections were still present with little latency change in a high-divalent cation solution (supplementary Fig. 1 and supplementary text, available at www.jneurosci.org as supplemental material). We therefore concluded that the connections were monosynaptic.

Table 1. Properties of synaptic connections between *alx* neurons and motoneurons

Type of *alx* neurons	Latency (ms)	EPSP (mV)	Reliability	Presence of electrical coupling	Pharmacology CNQX/AP-5
Strong movement					
1	0.37 ± 0.15	1.9 ± 1.2	0.6	−	NA
2	0.48 ± 0.08	4.6 ± 2.7	1	−	NA
3	0.53 ± 0.08	2.5 ± 0.6	0.9	−	NA
4	0.60 ± 0.08	1.3 ± 0.8	0.5	+	NA
5	0.57 ± 0.13	0.6 ± 0.4	1	+	NA
6	0.49 ± 0.10	1.3 ± 0.3	0.5	+	NA
7	0.56 ± 0.08	1.2 ± 0.4	0.2	−	NA
8	0.39 ± 0.06	1.9 ± 0.8	0.9	+	NA
9	0.37 ± 0.04	3.2 ± 0.4	0.4	−	NA
10	0.65 ± 0.06	1.8 ± 0.8	0.1	−	Blocked
11	0.28 ± 0.04	4.9 ± 1.2	1	+	Blocked
12	0.41 ± 0.05	3.0 ± 0.6	1	+	Blocked
13	0.37 ± 0.03	1.6 ± 0.4	1	−	Blocked
14	0.27 ± 0.04	4.1 ± 0.9	1	+	Blocked
15	0.34 ± 0.06	1.0 ± 0.4	1	+	NA
16	0.34 ± 0.06	5.0 ± 0.4	1	+	NA
17	0.45 ± 0.06	2.0 ± 0.6	0.8	+	NA
18	0.44 ± 0.09	1.7 ± 0.6	0.8	−	NA
19	0.52 ± 0.09	2.9 ± 1.8	1	+	NA
20	0.61 ± 0.13	2.2 ± 1.1	0.2	−	NA
21	0.43 ± 0.08	1.6 ± 1.0	0.5	+	NA
22	0.53 ± 0.14	3.2 ± 1.1	0.2	+	NA
Weak movement					
23	0.49 ± 0.06	1.0 ± 0.2	0.3	+	NA

For calculating each statistical value (latency, EPSP amplitude, reliability of synaptic connections), 10 events were used. Sometimes, multiple spikes were elicited during a single current injection. In these cases, we only used the first EPSP to measure the latency and EPSP amplitude for that current pulse (failures were not included). For measurements of synaptic reliability, the postsynaptic response that corresponded to the first presynaptic action potential after each current injection was used. Connection 5 was used to Figure 9*C*, 8 for Figure 9*B*, 9 for Figure 9*A*, 14 for Figure 10, and 23 for Figure 9*D*.

Our previous *in situ* hybridization results strongly suggested that *alx* neurons are glutamatergic. Consistent with this, the PSPs were blocked by the coapplication of CNQX (10 μM) and D-AP-5 (50 μM) in all five pairs tested (Table 1, Fig. 10). This further supported the notion that the connections were indeed glutamatergic (in these pharmacological experiments, the electrical components of the PSPs were not eliminated in mixed synapses; see below).

In addition to chemical synapses, we observed electrical coupling between *alx* neurons and motoneurons (18 of 47 pairs; the number includes mixed synapses; see below). The coupling coefficient varied from pair to pair (ranging from 1 to 6%). When it was high, electrical components of PSPs associated with the spikes of *alx* neurons were clearly observed. These electrical PSPs were characterized by ultra-fast transmission (Fig. 9*Be*, arrowhead). In all tested cases ($n = 10$), the presence of electrical coupling for pairs of ultra-fast transmission was supported by experiments in which subthreshold-depolarizing or hyperpolarizing somatic current injection in *alx* cells evoked depolarization or hyperpolarization of motoneurons, respectively. In two cases, such experiments were performed in the presence of TTX (data not shown). Among the 18 pairs having electrical connections, 13 of them were actually mixed (electrical and chemical) synapses. These mixed synapses were characterized by their dual-component PSPs: one displayed ultra-fast transmission, whereas the other exhibited fast transmission similar to monosynaptic chemical synapses (latencies of 0.3–0.7 ms). Figure 9, *Bd* and *Be*, shows a representative example. The PSPs associated with the spikes of the *alx* neurons had dual-component PSPs (arrow and arrowhead). In three cases, we tested the pharmacology of the mixed synapses, and only the chemical component was sensitive to CNQX/AP-5 treatment (Fig. 10), indicating that it was mediated by glutamatergic transmission. In the mixed synapses, chemical components sometimes failed to occur (Table 1). In contrast, electrical transmission never failed to occur.

In our paired recordings, we preferentially recorded from secondary motoneurons (ventrally located neurons of smaller size) that regularly fired during swimming (Fig. 9*Ab*). However, a small fraction of our data included paired recordings between *alx* neurons and primary motoneurons. The criteria for identifying primary motoneurons in this study were: (1) relatively dorsally located, (2) relatively large in soma size, and (3) only active during strong movements. In one case, a connection was found between a strong movement *alx* neuron and a primary motoneuron (Fig. 9*C*). Thus, strong movement type *alx* neurons were shown to make synaptic connections onto both primary and secondary motoneurons.

We also sought synaptic connections between weak-movement-type *alx* neurons and motoneurons. From 16 paired recordings, we found one pair that had a chemical connection (Fig. 9*D*). In this example, the PSPs had two components (Fig. 9*Dd*), indicating that the connection was a mixed synapse (Fig. 9*Dd*). We found four other pairs with electrical coupling, but

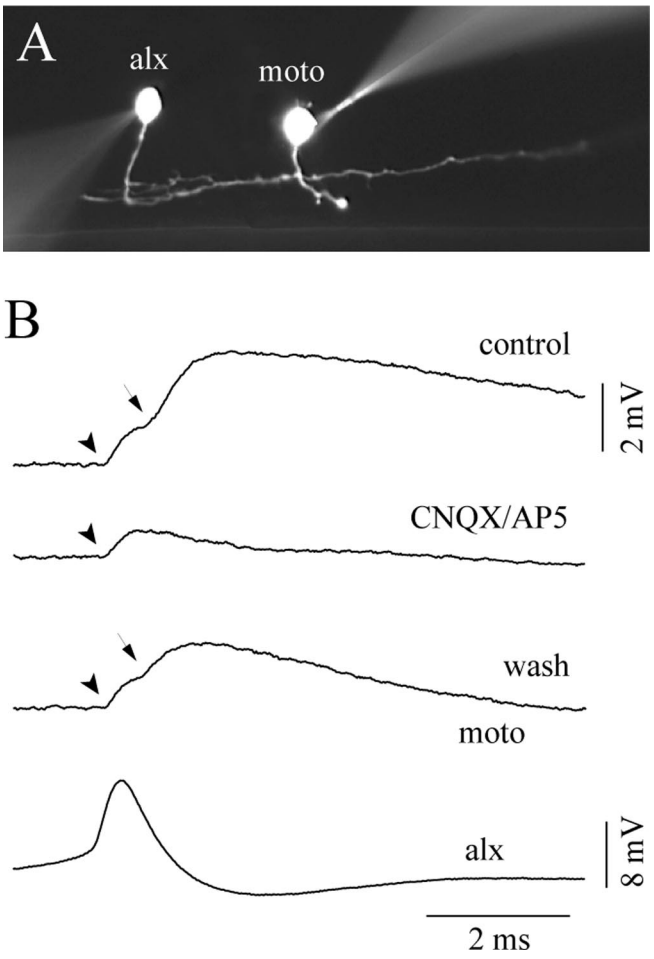

Figure 10. Pharmacology in a paired recording between an *alx* neuron and a motoneuron (moto). ***A***, A photo image of the recorded cells. ***B***, Pharmacology experiment. The top trace (control) shows that the EPSP has dual components (electrical, arrowhead; chemical, arrow). The second trace (CNQX/AP-5) shows that the chemical component of the EPSP was eliminated by the coapplication of CNQX (10 μM) and D-AP-5 (50 μM). The third trace (wash) shows that the chemical component reappeared after a washout of the drugs.

none of them appeared to have chemical components. Thus, the frequency of chemical connections between weak-movement-type *alx* neurons and motoneurons (1 of 16) appeared much lower than the connections between strong-movement-type *alx* neurons and motoneurons (22 of 47).

Discussion

Studies in En1-positive neurons in both aquatic anamniotic vertebrates and amniotes share common primary axonal trajectories, transmitter phenotype, and physiological roles in motor circuits (Saueressig et al., 1999; Wenner et al., 2000; Higashijima et al., 2004a; Li et al., 2004; Sapir et al., 2004; Goulding and Pfaff, 2005; Gosgnach et al., 2006). Here, we have extended our analysis to neurons marked by *alx*, a zebrafish homolog of *Chx10.* We found that *alx* neurons have primarily descending axons and are glutamatergic. Therefore, as with En1 neurons, we found a clear link between *alx* expression and both the morphology and transmitter phenotype of the neurons. Because a*lx* marks ipsilateral descending glutamatergic neurons in zebrafish, we expect that Chx10 neurons in amniotes may also be glutamatergic neurons whose primary axonal trajectories are ipsilateral and descending. Consistent with this, Chx10-positive neurons in mice are labeled by the application of a dextran-conjugated dye caudal and ipsilateral to their somata in the spinal cord (Thaler et al., 1999). Recently, it has been shown that neurons that express the EphA4 tyrosine kinase receptor are important for mammalian locomotion (Kullander et al., 2003) and that a subset of these neurons excite motoneurons on the same side (Butt et al., 2005). These ipsilateral excitatory neurons might overlap with Chx10-positive neurons.

Whereas En1 neurons in zebrafish represented a single functional cell type (Higashijima et al., 2004a; Li et al., 2004), there appeared to be heterogeneity among *alx* neurons. Dorsally located neurons tended to be more involved in strong movements, whereas ventrally located ones tended to be more involved in regular swimming. The presence of heterogeneity is perhaps not surprising. One emerging view is that the early V0–V3 subdivision of neurons in the embryonic spinal cord represents a primitive developmental ground state that undergoes further diversification during development (Goulding and Pfaff, 2005). In amniotes, V2 neurons are subdivided into at least Chx10-positive V2a and Gata2/3-positive V2b neurons (Karunaratne et al., 2002). This subdivision may also be present in zebrafish (see below). In addition, *alx* neurons themselves will undergo diversification early in development, whereas diversification of V1 neurons may be delayed. In amniotes, V1 neurons clearly show diversification and contain a minimum of two different cell types, Renshaw cells and Ia inhibitory neurons (Sapir et al., 2004; Alvarez et al., 2005).

It is not clear whether V2a and V2b subdivision is present in zebrafish. If such a subdivision is present, the prime candidates for V2b neurons are the ipsilateral descending neurons that were negative for *alx* (Fig. 6*C*). This point awaits the analysis of gata2/3-positive neurons in zebrafish (Neave et al., 1995).

How heterogeneity among *alx* neurons is established during development is unknown. The ventricular zone changes its properties during development. Cells that derive from a particular domain early in development could differ from those born at later stages (Marquardt and Pfaff, 2001). Because a difference in the properties of *alx* neurons correlates with the birth date of the neurons, this could be the case here. Alternatively, the difference may arise from the influence of the environment after the neurons settle in their final position. Earlier-born *alx* neurons settle more dorsally, where they could receive different extrinsic signals. Such signals could help establish the properties of the strong class *alx* neurons.

In zebrafish, En1 neurons are ipsilateral ascending inhibitory neurons, whereas *alx* neurons are ipsilateral descending excitatory neurons. This configuration, ascending inhibition and descending excitation, is suitable for producing undulatory movement in which activity shifts from rostral to caudal along the same side of the body. The ancient vertebrate, which most likely used undulatory movement for locomotion, might have also adopted this configuration. Using this evolutionary framework, current vertebrate species, including mammals, may have evolved more complex systems. This might explain why the primary axonal trajectories of local inhibitory neurons such as Renshaw cells and Ia inhibitory neurons are ascending during development (Saueressig et al., 1999).

Our studies have shown that *alx* neurons are involved in escape behavior. The escape behavior is initiated by the Mauthner neuron in the brainstem (Zottoli, 1977). In goldfish, Mauthner neurons make monosynaptic excitatory connections to both motoneurons and ipsilateral descending neurons, which themselves make monosynaptic excitatory connections onto motoneurons (Fetcho, 1991). Calcium imaging studies in zebrafish have shown

that CiD neurons, similar in morphology to the goldfish ipsilateral descending neurons, are activated during escapes (Ritter et al., 2001). Here, we demonstrated that CiD neurons are among *alx* neurons and provided evidence that the strong class *alx* neurons are activated during escapes. We also provided evidence that these neurons make frequent monosynaptic excitatory connections onto motoneurons (22 of 47 pairs were chemically connected). These results, together with the calcium imaging studies, suggest that the strong class *alx* neurons correspond to the interneurons activated by Mauthner, as first identified in goldfish.

One suggested role of this polysynaptic pathway is to amplify the excitation at the level of the spinal cord, thereby resulting in a massive activation of motoneurons on one side of the body (Fetcho and O'Malley, 1995). We have shown that the strong class *alx* neurons make synapses onto both primary and secondary motoneurons. A connection of the former is known in goldfish (Fetcho, 1992), but we are the first to describe the latter connection. No other source of excitation has been demonstrated for the activation of secondary motoneurons during escapes. Thus, the excitation coming from *alx* neurons may account for most of the excitation that secondary motoneurons receive during escapes.

Ipsilateral descending excitatory neurons play important roles in the central pattern generator (CPG) for swimming behavior in tadpoles and lampreys, serving as the main source of on-cycle excitation. This notion comes from many lines of evidence including lesions, pharmacology, and paired recordings (Roberts et al., 1998; Buchanan, 2001). These neurons are rhythmically active in phase with ventral root activity and make glutamatergic excitatory connections onto motoneurons (Dale and Roberts, 1985; Buchanan and Grillner, 1987). We have shown that ventrally located *alx* neurons are rhythmically active during swimming in phase with the activity of nearby motoneurons. Assuming that neural circuits generating swimming are similar in all aquatic vertebrates, these *alx* neurons are prime candidates for excitatory neurons in the CPG in zebrafish. Consistent with this, we found excitatory synaptic connections between weak class *alx* neurons and motoneurons. Therefore, we presume that these neurons contribute to on-cycle excitation during slow swimming. We need to note, however, that our evidence on this point is limited. The number of connection we found was just one of 16 pairs. In addition, there are ipsilateral descending neurons that were negative for *alx*, and these neurons might play more important roles during swimming.

alx neurons are approximately categorized into two groups based on their activity. It is not clear whether such a subdivision is present in tadpoles/lampreys. Tadpoles produce very strong movements, termed struggling. Soffe (1993) has shown that the same ipsilateral descending neurons are recruited both in swimming and struggling. However, it is still possible that there exist ipsilateral descending neurons that are only recruited for struggling.

Although many of the *alx* neurons of the weak class were also recruited into strong movements, some of them were not (Fig. 8*C*). This finding is interesting with respect to the extent with which neurons of a particular type participate in a given motor behavior. In general, movements can occur with several different forms or different strengths, but the basis of how this difference is encoded by the nervous system remains essentially unknown, especially at the interneuronal level. Escape, fast swimming, and slow swimming all involve sequential contractions of body muscles. The simplest scenario is that stronger movements are the result of more recruited neurons. However, a calcium imaging study in zebrafish (Ritter et al., 2001) has shown that two different populations of interneurons, multipolar commissural descending (MCoD) neurons and CiD neurons, are differentially activated during two different behaviors (slow swimming and escape). Thus, at least at some level, a switching in the interneuronal population occurs. Our study suggests that such switching occurs not only between two completely different populations (MCoD vs CiD) but also between closely related neurons (strong movement vs weak movement *alx* neurons).

The development of the strong class of *alx* neurons precedes that of the weak class. Interestingly, this parallels the behavioral development of zebrafish. At earlier developmental stages (17–28 hpf), zebrafish embryos only show strong contraction movements, a movement that is somewhat similar to escapes. Swimming movements appear later and gradually mature between 30 and 2–3 dpf. Therefore, the development of swimming type *alx* neurons could be one of the main factors that enable the animal to perform swimming behavior.

Finally, we found electrical coupling between *alx* neurons and motoneurons. Many spinal neurons are electrically coupled at very early stages (Saint-Amant and Drapeau, 2001). Such network-wide electrical coupling is likely to diminish as animals mature. The coupling we observed could be a remnant of early coupling and might subsequently disappear. However, electrical coupling is also present in the adult CNS (Bennett et al., 1963; Ringham, 1975). Indeed, electrical connections between ipsilateral descending neurons and primary motoneurons are documented in the spinal cord of adult goldfish (Fetcho, 1992). One significance of electrical coupling is its fast transmission, which is important for producing quick responses such as escapes. Therefore, it is likely that some of the electrical connections we observed would remain in adults.

References

Alvarez FJ, Jonas PC, Sapir T, Hartley R, Berrocal MC, Geiman EJ, Todd AJ, Goulding M (2005) Postnatal phenotype and localization of spinal cord V1 derived interneurons. J Comp Neurol 493:177–192.

Ando R, Hama H, Yamamoto-Hino M, Mizuno H, Miyawaki A (2002) An optical marker based on the UV-induced green-to-red photoconversion of a fluorescent protein. Proc Natl Acad Sci USA 99:12651–12656.

Barabino SM, Spada F, Cotelli F, Boncinelli E (1997) Inactivation of the zebrafish homologue of Chx10 by antisense oligonucleotides causes eye malformations similar to the ocular retardation phenotype. Mech Dev 63:133–143.

Bennett MVL, Aljure E, Nakajima Y, Pappas GD (1963) Electrotonic junctions between teleost spinal neurons: electrophysiology and ultrastructure. Science 141:262–264.

Bernhardt RR, Chitnis AB, Lindamer L, Kuwada JY (1990) Identification of spinal neurons in the embryonic and larval zebrafish. J Comp Neurol 302:603–616.

Bhatt DH, Otto SJ, Depoister B, Fetcho JR (2004) Cyclic AMP-induced repair of zebrafish spinal circuits. Science 305:254–258.

Briscoe J, Pierani A, Jessell TM, Ericson J (2000) A homeodomain protein code specifies progenitor cell identity and neuronal fate in the ventral neural tube. Cell 101:435–445.

Buchanan JT (2001) Contributions of identifiable neurons and neuron classes to lamprey vertebrate neurobiology. Prog Neurobiol 63:441–466.

Buchanan JT, Grillner S (1987) Newly identified 'glutamate interneurons' and their role in locomotion in the lamprey spinal cord. Science 236:312–314.

Butt SJ, Lundfald L, Kiehn O (2005) EphA4 defines a class of excitatory locomotor-related interneurons. Proc Natl Acad Sci USA 102:14098–14103.

Campbell RE, Tour O, Palmer AE, Steinbach PA, Baird GS, Zacharias DA, Tsien RY (2002) A monomeric red fluorescent protein. Proc Natl Acad Sci USA 99:7877–7882.

Dale N, Roberts A (1985) Dual-component amino-acid-mediated synaptic potentials: excitatory drive for swimming in *Xenopus* embryos. J Physiol (Lond) 363:35–59.

Drapeau P, Ali DW, Buss RR, Saint-Amant L (1999) In vivo recording from identifiable neurons of the locomotor network in the developing zebrafish. J Neurosci Methods 88:1–13.

Ericson J, Rashbass P, Schedl A, Brenner-Morton S, Kawakami A, van Heyningen V, Jessell TM, Briscoe J (1997) Pax6 controls progenitor cell identity and neuronal fate in response to graded Shh signaling. Cell 90:169–180.

Fetcho JR (1991) Spinal network of the Mauthner cell. Brain Behav Evol 37:298–316.

Fetcho JR (1992) Excitation of motoneurons by the Mauthner axon in goldfish: complexities in a "simple" reticulospinal pathway. J Neurophysiol 67:1574–1586.

Fetcho JR, O'Malley DM (1995) Visualization of active neural circuitry in the spinal cord of intact zebrafish. J Neurophysiol 73:399–406.

Frankenhaeuser B, Hodgkin AL (1957) The action of calcium on the electrical properties of squid axons. J Physiol (Lond) 137:218–244.

Gosgnach S, Lanuza GM, Butt SJ, Saueressig H, Zhang Y, Velasquez T, Riethmacher D, Callaway EM, Kiehn O, Goulding M (2006) V1 spinal neurons regulate the speed of vertebrate locomotor outputs. Nature 440:215–219.

Goulding M, Pfaff SL (2005) Development of circuits that generate simple rhythmic behaviors in vertebrates. Curr Opin Neurobiol 15:14–20.

Goulding M, Lanuza G, Sapir T, Narayan S (2002) The formation of sensorimotor circuits. Curr Opin Neurobiol 12:508–515.

Grillner S (2003) The motor infrastructure: from ion channels to neuronal networks. Nat Rev Neurosci 4:573–586.

Gu H, Marth JD, Orban PC, Mossmann H, Rajewsky K (1994) Deletion of a DNA polymerase beta gene segment in T cells using cell type-specific gene targeting. Science 265:103–106.

Hale ME, Ritter DA, Fetcho JR (2001) A confocal study of spinal interneurons in living larval zebrafish. J Comp Neurol 437:1–16.

Hieber V, Dai X, Foreman M, Goldman D (1998) Induction of alpha1-tubulin gene expression during development and regeneration of the fish central nervous system. J Neurobiol 37:429–440.

Higashijima S, Okamoto H, Ueno N, Hotta Y, Eguchi G (1997) High-frequency generation of transgenic zebrafish which reliably express GFP in whole muscles or the whole body by using promoters of zebrafish origin. Dev Biol 192:289–299.

Higashijima S, Masino MA, Mandel G, Fetcho JR (2004a) Engrailed-1 expression marks a primitive class of inhibitory spinal interneuron. J Neurosci 24:5827–5839.

Higashijima S, Mandel G, Fetcho JR (2004b) Distribution of prospective glutamatergic, glycinergic, and GABAergic neurons in embryonic and larval zebrafish. J Comp Neurol 480:1–18.

Higashijima S, Schaefer M, Fetcho JR (2004c) Neurotransmitter properties of spinal interneurons in embryonic and larval zebrafish. J Comp Neurol 480:19–37.

Jankowska E (1992) Interneuronal relay in spinal pathways from proprioceptors. Prog Neurobiol 38:335–378.

Karunaratne A, Hargrave M, Poh A, Yamada T (2002) GATA proteins identify a novel ventral interneuron subclass in the developing chick spinal cord. Dev Biol 249:30–43.

Kiehn O, Butt SJ (2003) Physiological, anatomical and genetic identification of CPG neurons in the developing mammalian spinal cord. Prog Neurobiol 70:347–361.

Kullander K, Butt SJ, Lebret JM, Lundfald L, Restrepo CE, Rydstrom A, Klein R, Kiehn O (2003) Role of EphA4 and EphrinB3 in local neuronal circuits that control walking. Science 299:1889–1892.

Kuwada JY, Bernhardt RR, Nguyen N (1990) Development of spinal neurons and tracts in the zebrafish embryo. J Comp Neurol 302:617–628.

Lee EC, Yu D, Martinez de Velasco J, Tessarollo L, Swing DA, Court DL, Jenkins NA, Copeland NG (2001) A highly efficient *Escherichia coli*-based chromosome engineering system adapted for recombinogenic targeting and subcloning of BAC DNA. Genomics 73:56–65.

Li WC, Higashijima S, Parry DM, Roberts A, Soffe SR (2004) Primitive roles for inhibitory interneurons in developing frog spinal cord. J Neurosci 24:5840–5848.

Marquardt T, Pfaff SL (2001) Cracking the transcriptional code for cell specification in the neural tube. Cell 106:651–654.

Masino MA, Fetcho JR (2005) Fictive swimming motor patterns in wild type and mutant larval zebrafish. J Neurophysiol 93:3177–3188.

Neave B, Rodaway A, Wilson SW, Patient R, Holder N (1995) Expression of zebrafish GATA 3 (gta3) during gastrulation and neurulation suggests a role in the specification of cell fate. Mech Dev 51:169–182.

Ringham GL (1975) Localization and electrical characteristics of a giant synapse in the spinal cord of the lamprey. J Physiol (Lond) 251:395–407.

Ritter DA, Bhatt DH, Fetcho JR (2001) *In vivo* imaging of zebrafish reveals differences in the spinal networks for escape and swimming movements. J Neurosci 21:8956–8965.

Roberts A, Soffe SR, Wolf ES, Yoshida M, Zhao FY (1998) Central circuits controlling locomotion in young frog tadpoles. Ann NY Acad Sci 860:19–34.

Sagne C, El Mestikawy S, Isambert MF, Hamon M, Henry JP, Giros B, Gasnier B (1997) Cloning of a functional vesicular GABA and glycine transporter by screening of genome databases. FEBS Lett 417:177–183.

Saint-Amant L, Drapeau P (2001) Synchronization of an embryonic network of identified spinal interneurons solely by electrical coupling. Neuron 31:1035–1046.

Sander M, Paydar S, Ericson J, Briscoe J, Berber E, German M, Jessell TM, Rubenstein JL (2000) Ventral neural patterning by Nkx homeobox genes: Nkx6.1 controls somatic motor neuron and ventral interneuron fates. Genes Dev 14:2134–2139.

Sapir T, Geiman EJ, Wang Z, Velasquez T, Mitsui S, Yoshihara Y, Frank E, Alvarez FJ, Goulding M (2004) Pax6 and engrailed 1 regulate two distinct aspects of renshaw cell development. J Neurosci 24:1255–1264.

Saueressig H, Burrill J, Goulding M (1999) Engrailed-1 and netrin-1 regulate axon pathfinding by association interneurons that project to motor neurons. Development 126:4201–4212.

Sharma K, Sheng HZ, Lettieri K, Li H, Karavanov A, Potter S, Westphal H, Pfaff SL (1998) LIM homeodomain factors Lhx3 and Lhx4 assign subtype identities for motor neurons. Cell 95:817–828.

Soffe SR (1993) Two distinct rhythmic motor patterns are driven by common premotor and motor neurons in a simple vertebrate spinal cord. J Neurosci 13:4456–4469.

Thaler J, Harrison K, Sharma K, Lettieri K, Kehrl J, Pfaff SL (1999) Active suppression of interneuron programs within developing motor neurons revealed by analysis of homeodomain factor HB9. Neuron 23:675–687.

Thermes V, Grabher C, Ristoratore F, Bourrat F, Choulika A, Wittbrodt J, Joly JS (2002) I-SceI meganuclease mediates highly efficient transgenesis in fish. Mech Dev 118:91–98.

Wenner P, O'Donovan MJ, Matise MP (2000) Topographical and physiological characterization of interneurons that express engrailed-1 in the embryonic chick spinal cord. J Neurophysiol 84:2651–2657.

Zottoli SJ (1977) Correlation of the startle reflex and Mauthner cell auditory responses in unrestrained goldfish. J Exp Biol 66:243–254.